HUMAN GENETICS

Inhibiting EZH2 complements steroid effects in Duchenne muscular dystrophy

Eun Young Jeon[1], Yejin Kwak[2], Hyeji Kang[1,3], Hanbyeol Kim[1,3], Se Young Jin[4], Soojin Park[5], Ryeo Gyeong Kim[6], Dayoung Ko[7], Jae-Kyung Won[8], Anna Cho[6], Inkyung Jung[4], Chul-Hwan Lee[1,3,9], Jeongbin Park[2,10], Hyun-Young Kim[7], Jong-Hee Chae[5,11]*†, Murim Choi[1]*†

Duchenne muscular dystrophy (DMD) is a devastating X-linked disorder caused by dystrophin gene mutations. Despite recent advances in understanding the disease etiology and applying emerging treatment methodologies, glucocorticoid derivatives remain the only general therapeutic option that can slow disease development. However, the precise molecular mechanism of glucocorticoid action remains unclear, and there is still need for additional remedies to complement the treatment. Here, using single-nucleus RNA sequencing and spatial transcriptome analyses of human and mouse muscles, we investigated pathogenic features in patients with DMD and palliative effects of glucocorticoids. Our approach further illuminated the importance of proliferating satellite cells and revealed increased activity of a signal transduction pathway involving EZH2 in the patient cells. Subsequent administration of EZH2 inhibitors to *Dmd* mutant mice resulted in improved muscle phenotype through maintaining the immune-suppressing effect but overriding the muscle weakness and fibrogenic effects exerted by glucocorticoids. Our analysis reveals pathogenic mechanisms that can be readily targeted by extant therapeutic options for DMD.

INTRODUCTION

Duchenne muscular dystrophy (DMD) is a severe, progressive muscle-wasting X-linked genetic disorder that affects about 1 in 5000 males (*1*). Mutations in the dystrophin gene are responsible for both DMD and Becker muscular dystrophy (BMD), a relatively less severe and heterogeneous form of dystrophinopathy (*2*). The severe symptoms of DMD and relative ease of access to the affected tissue made it one of the first target diseases for emerging cell- and gene-based therapeutic approaches. However, attempts involving viral transfer of the *DMD* gene or gene activation machinery via the clustered regularly interspaced short palindromic repeats (CRISPR) system have yielded unsatisfactory outcomes (*3*–*5*). Therefore, although studies have demonstrated that gene editing therapies can positively affect patients and early data suggest that the therapy has the potential to restore dystrophin protein production (*6*), challenges remain in validating the clinical benefits and controlling potential off-target effects that need to be addressed before clinical application (*7*).

At present, the standard of care for DMD still relies on glucocorticoids (e.g., deflazacort and prednisone), mitigating the disease progression by reducing inflammation-induced muscle damage, which minimizes muscle strength loss (*8*–*10*). Treatment with deflazacort delays the onset of cardiomyopathy in patients with DMD until the age of 18 and increases patient survival by over 5 to 15 years (*11*). However, the precise action of deflazacort in DMD muscle tissue is still unclear, and its long-term administration has well-documented side effects such as obesity, behavioral changes, short stature, and osteopenia (*12*). There have been a few attempts to treat DMD using a chemical compound; for example, cyclosporine is administered as an immunosuppressant (*13*, *14*), suramin attenuates cardiac dysfunction in a DMD mouse model (*15*), and forskolin has improved muscle performance and regenerative capacities in a DMD rat model (*16*). However, although these experimental treatments show promise, it remains crucial to continue pursuing for more effective and safely approved drugs for DMD; in particular, a therapeutic that complements deflazacort function would be of great benefit to patients with DMD.

Now, four antisense oligonucleotides (ASOs) that are designed to induce skipping of exon 45, 51, or 53 of dystrophin have been granted conditional approval by the Food and Drug Administration (FDA) (*1*, *17*, *18*). However, the ASO method is specific to particular *DMD* mutations and therefore shows limited applicability. Recently, the FDA also approved minigene therapy for the treatment of pediatric patients with ambulatory DMD (*3*). However, a clinical benefit such as enhanced motor function has not been confirmed, and the FDA has mandated the company to conduct a comprehensive clinical study to validate the drug's clinical advantages as a condition for maintaining approval (*4*). Moreover, even patients successfully treated with these approaches will still be administered steroids as part of standard care. Therefore, there is still critical need for a therapeutic method that can be applied on a broad range of patients with DMD and complement steroids.

Satellite cells constitute a heterogeneous population of stem cells that play indispensable roles in the development, preservation, and regenerative processes of skeletal muscles (*19*). These cells can be distinguished by expression of the transcription factor paired-box 7 (PAX7), which has the critical role of enforcing the myogenic program within them (*20*). In DMD, the absence of dystrophin expression leads

[1]Department of Biomedical Sciences, Seoul National University College of Medicine, Seoul, Republic of Korea. [2]Department of Information Convergence Engineering, Pusan National University, Yangsan, Republic of Korea. [3]Department of Pharmacology, Seoul National University College of Medicine, Seoul, Republic of Korea. [4]Department of Biological Sciences, Korea Advanced Institute of Science and Technology (KAIST), Daejeon, Republic of Korea. [5]Department of Genomic Medicine, Seoul National University Hospital, Seoul, Republic of Korea. [6]Department of Pediatrics, Rare Disease Center, Seoul National University Bundang Hospital, Gyeonggi-do, Republic of Korea. [7]Department of Pediatric Surgery, Seoul National University Children's Hospital, Seoul, Republic of Korea. [8]Department of Pathology, Seoul National University Hospital, Seoul National University College of Medicine, Seoul, Republic of Korea. [9]Cancer Research Institute, Seoul National University College of Medicine, Seoul, Republic of Korea. [10]School of Biomedical Convergence Engineering, Pusan National University, Yangsan, Republic of Korea. [11]Department of Pediatrics, Seoul National University College of Medicine, Seoul, Republic of Korea.
*Corresponding author. Email: murimchoi@snu.ac.kr (M.C.); chaeped1@snu.ac.kr (J.-H.C.)
†These authors contributed equally to this work.

to impaired regeneration and exacerbating muscle wasting (*21*). In addition to PAX7, polycomb repressive complex 2 (PRC2) has a crucial role in regulating stem-like processes in satellite cells; in cultured skeletal muscle cells, it regulates the cell cycle by controlling proliferation through methylation of histone 3 lysine 27 (H3K27me3). In particular, elevated expression of its histone methyltransferase subunit Ezh2 in cultured mouse cells has been shown to inhibit muscle differentiation (*22*). Therefore, perturbation of EZH2 in satellite cells may provide an opportunity for influencing myocyte differentiation in skeletal muscle.

To further understand the cellular and molecular mechanism of deflazacort in DMD and to suggest additional therapeutic options for the disease, we performed a comparative analysis of human patients with DMD and BMD and *Dmd* mutant mice with or without deflazacort treatment using single-nucleus RNA sequencing (snRNA-seq). This study design intended selective utilization of human and mouse systems in modeling DMD and steroid treatment. Spatial transcriptomics were used to observe cell-cell interactions, particularly highlighting how immune cells in close proximity to other cell types may influence these mechanisms, affecting disease progression. Subsequently, we reveal disease-specific features in DMD muscle tissues and demonstrate molecular mechanisms underlying the beneficial effects of deflazacort, as well as potential therapeutic strategies for using EZH2 inhibitors, GSK126 and tazemetostat, to improve muscle phenotype in combination with glucocorticoids. The beneficial effect was found not only in satellite cells but also in other cell types, such as immune cells and fibro-adipogenic progenitors (FAPs). Ultimately, our results elucidate a compensatory mechanism of stem cell stimulation on the established effect of deflazacort.

RESULTS

Cellular profiles of muscle tissues in human cases and a DMD mouse model

snRNA-seq was performed on fresh frozen quadriceps femoris obtained from three male individuals with DMD, three male individuals with BMD, and five healthy control individuals (Materials and Methods; Fig. 1A, fig. S1, and table S1). Among the control samples, three were derived from abdominal muscle tissue. All participants were under the age of 17, and each group was composed of individuals of similar ages. Of the patients with BMD, two exhibited deletion mutations (p.Glu2147_Gln2171del and exon 30-42 del), whereas the third had a stop codon mutation (p.Ser1273X) in dystrophin gene. Among the DMD cases, two had stop codon mutations (p.Arg195X and p.Gln423X), and one patient had a frameshift insertion mutation (p.His3299Glnfs*15) (table S1). Following snRNA-seq of these muscle samples, quality filtering was performed and 60,884 nuclei were retained for subsequent analyses. We captured 11 main cell types, including type I and II muscle cells, FAPs, satellite cells, and myeloid cells (Fig. 1B and tables S2 and S3). Notably, patients with BMD and DMD exhibited expansion of FAP and myeloid lineages, concomitant with a decline in muscle fiber populations (Fig. 1, C and D; fig. S2; and data S1). The proportion of immune cells in BMD did not show a notable difference from controls.

We also performed snRNA-seq on fresh frozen muscle cells from two male wild-type DBA/2J mice, two male D2.B10-*DMD*^{mdx}/J (or D2-mdx) mice, and two male D2-mdx mice administered with deflazacort (Materials and Methods; Fig. 1A and fig. S1). The two mice in each genotype group consist of a 7- and a 28-week-old mouse as D2-mdx mice show a notable decline in skeletal muscle function as early as 7 weeks and in cardiac function by 28 weeks (*23*). Seven distinct cell types were identified from 20,899 nuclei (Fig. 1E and table S4). Like human patient muscles, D2-mdx muscles exhibited a decrease in muscle fiber and an increase in myeloid and lymphoid cell subpopulations (Fig. 1, F and G). In D2-mdx animals subjected to deflazacort treatment, noticeable reduction in myeloid cell frequencies and increase in muscle fiber were evident. Inflammatory myeloid cell population marked by *Cd44* and *Itgam* genes drove this change (fig. S2). In the comparative analysis between 7- and 28-week-old mice, we repeatedly observed a notable increase in Wnt signaling gene expression. The hallmark was up-regulation of *Tcf7l2*, a transcription factor for Wnt signaling, target genes of which were confirmed to have increased expression in 7-week-old D2-mdx mice as assayed by single-cell regulatory network inference and clustering (SCENIC) (fig. S3). This observation was not seen in wild-type mice or in D2-mdx mice given deflazacort. Notably, deflazacort administered to the 7-week mouse was able to efficiently revert the expression back to the wild-type mouse, whereas the 28-week mouse was less pronounced (fig. S4). These results support the presence of qualitative differences in different ages of muscles, and the glucocorticoid treatment is more efficient in the young, consistent with the previous studies (*24*–*26*).

Concurrently with the snRNA-seq profiling, spatial transcriptomics was conducted on the same three samples, consisting of two patients with DMD and one healthy sample, using the Visium method (Fig. 1H and figs. S1 and S5). The control subject showed mainly muscle-specific expression profiles, aligning with the observed cellular composition. However, the two slides derived from patients with DMD exhibited substantial augmentation of myeloid cell expression profiles, indicating a pronounced shift in the cellular landscape. Cell type co-occurrence analysis further demonstrated an increase in the co-occurrence of satellite cells, myeloid cells, and lymphoid cells, suggesting local interactions among these cells in the DMD muscle (Fig. 1, I and J).

Effects of deflazacort in humans and a mouse DMD model

To investigate the molecular consequences of deflazacort treatment in humans and mouse models of DMD, we conducted a comprehensive investigation of differentially expressed genes (DEGs). In myeloid cells, a cluster of guanine nucleotide exchange factors (GEFs) encompassing *DOCK2*, *DOCK8*, and *DOCK10* displayed substantial up-regulation across BMD, DMD, and D2-mdx mice when compared to corresponding controls (Fig. 2, A and B), implying up-regulation of RhoA-mediated actin remodeling, cell migration, and subsequent immune activation (*27*, *28*). Administration of deflazacort resulted in a decreased expression of these genes. Binding sites for NR3C1, a dedicated nuclear receptor for glucocorticoid, were identified near *DOCK2*, *DOCK8*, and *DOCK10* loci, with the addition of dexamethasone in A549 cells (*29*), suggesting that these genes can be direct downstream factors of deflazacort (Fig. 2C and fig. S6). We also performed Nr3c1 chromatin immunoprecipitation sequencing (ChIP-seq) in mouse myeloid RAW264.7 cells and revealed consistent results, showing Nr3c1 peaks in the target genes, Dock10, Dock8, and Dock2 (fig. S7).

Similarly, we investigated DEGs within lymphoid cells (Fig. 2D). Genes linked to hematopoiesis, B cell differentiation, survival, immunoglobulin (Ig) production, and the phosphatidylinositol 3-kinase to AKT to mammalian target of rapamycin (PI3K-AKT-mTOR)

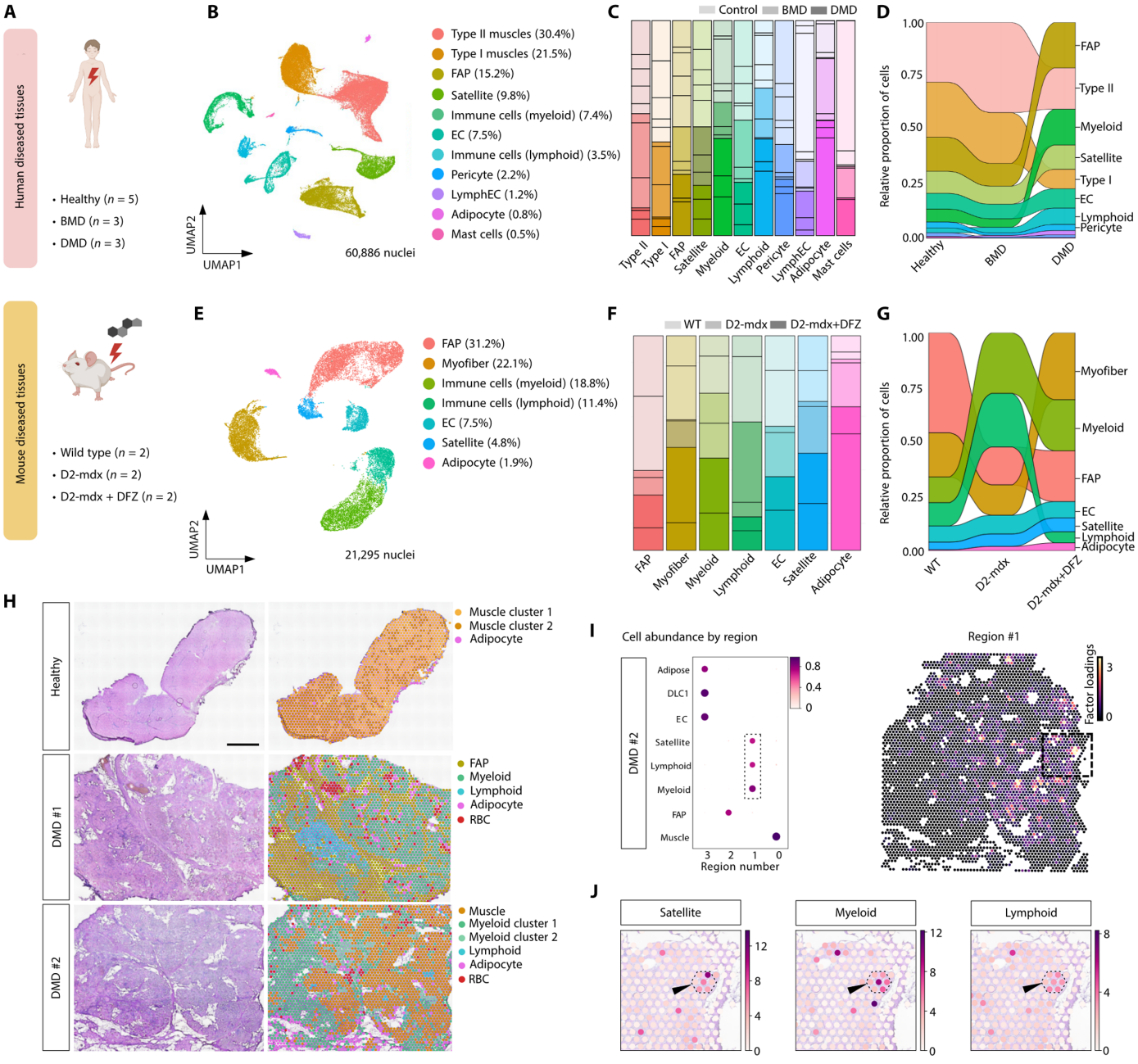

Fig. 1. Profiles of human and mouse DMD muscle tissues. (**A**) Human and mouse tissues used in the study. DFZ denotes deflazacort. (**B** and **E**) Uniform Manifold Approximation and Projection (UMAP) visualization of 60,886 nuclei from human (B) and 21,295 nuclei from mouse (E) tissues. FAP, fibro-adipogenic progenitors; EC, endothelial cells; LymphEC, lymphatic endothelial cells. (**C** and **F**) Cell type proportions in human (C) and mouse (F) samples. The five control samples are positioned in the uppermost bolded box of each column, highlighted in the brightest shade. The three BMD samples are situated in the middle bolded box, whereas the three DMD samples are located in the lowermost bolded box, shaded with the darkest color. WT, wild type. (**D** and **G**) Changes in cell type proportion by disease state in human (D) and mouse (G) samples. (**H**) Cell type mapping on Visium slides of human DMD and healthy muscle sections. Scale bar, 1 mm. (**I**) Dot plot illustrating co-occurrence of spatially resolved cell types in regions defined by cell2location (*78*). The dotted rectangle emphasizes the co-occurrence of satellite cells and immune cells in region #1 (left). Spatial heatmap showing the location of region #1 (right). (**J**) Magnified view of the dotted rectangle in (I) (right), emphasizing colocalized expression of satellite, myeloid, and lymphoid markers in the DMD #2 sample.

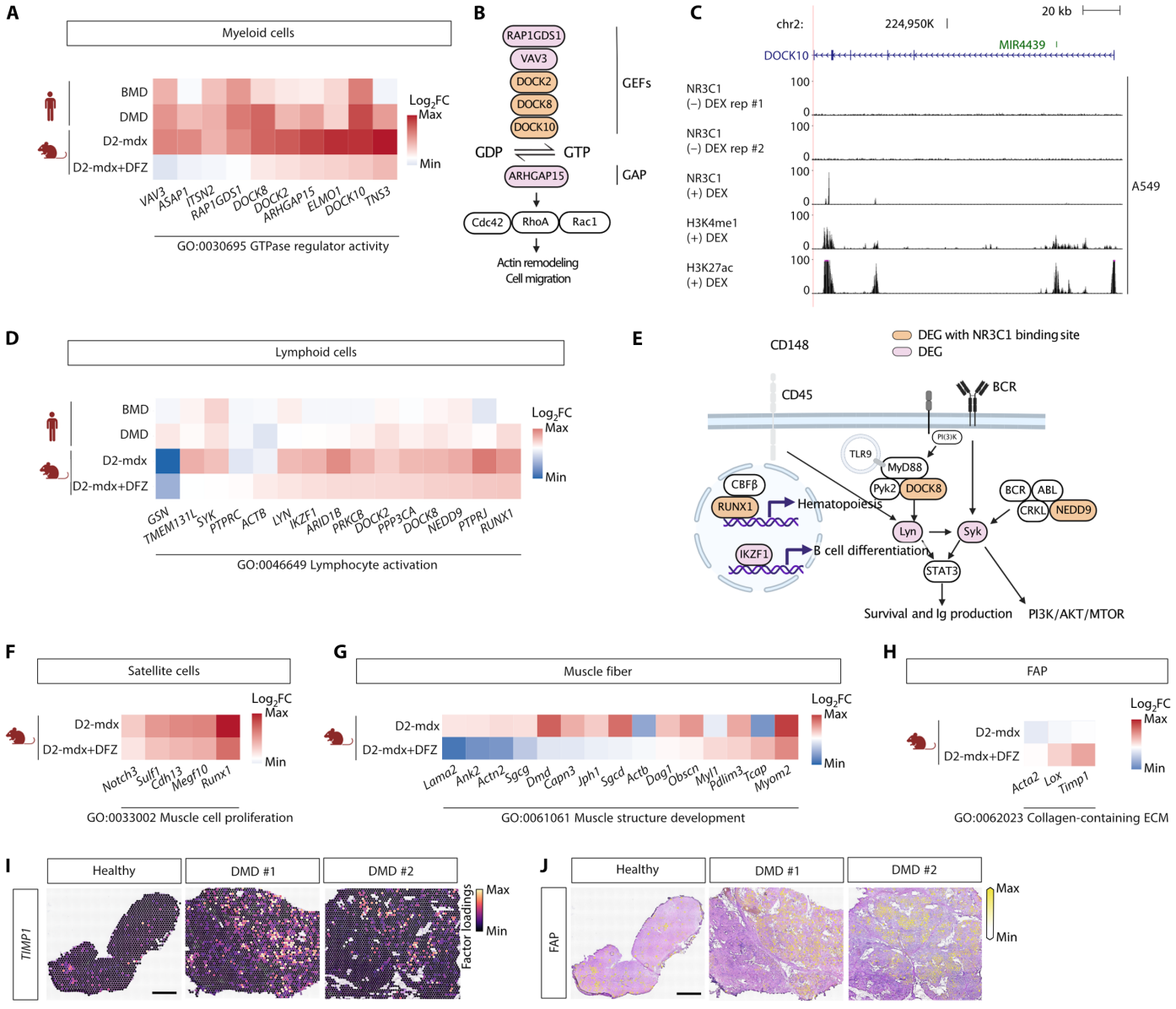

Fig. 2. Altered gene expression in human and mouse tissues with *DMD* mutation and deflazacort treatment. (**A**, **D**, **F**, **G**, and **H**) Heatmaps of DEGs in each cell type by species and disease status. (A) Myeloid cells. (D) Lymphoid cells. (F) Satellite cells. (G) Muscle cells. (H) FAP cells. FC, fold change; GTPase, guanosine triphosphatase; ECM, extracellular matrix. (**B** and **E**) Schematic representation of the roles of DEGs in corresponding heatmaps. (B) Actin remodeling and cell migration genes in myeloid cells. (E) B cell differentiation, survival, and Ig production genes in lymphoid cells. (**C**) Diagram of the exemplary NR3C1 ChIP-seq peak locus on *DOCK10*, a DEG found in the myeloid cells. DEX denotes dexamethasone. (**I**) *TIMP1* expression in FAP clusters. (**J**) Visualization of FAP clusters by cell2location mapping on Visium slides of human patient muscle sections. Scale bars, 1 mm.

pathway exhibited increased expression across BMD, DMD, and D2-mdx lymphocytes (Fig. 2E). Upon deflazacort administration, expression of these genes was attenuated (Fig. 2D).

In contrast to the discernible improvements seen in myeloid and lymphoid cells following deflazacort intervention, no enhancement was observed within satellite, muscle, and FAP clusters (Fig. 2, F to H). Genes related to regulation of satellite cell growth and muscle regeneration were depleted (Fig. 2F) (*30*–*33*), and muscle structural genes (Fig. 2G) displayed decreased expression following deflazacort administration. The concomitant elevated presence of profibrotic FAP markers (Fig. 2, H and I) suggests a potential avenue for intervention as FAP cells are capable of differentiating toward either adipogenic or myofibroblast lineages (Fig. 2J) (*34*, *35*). Therefore, although deflazacort positively affects immune cells through controlling inflammatory signaling pathways, it also exacerbates muscle structure deficits and fibrosis in DMD muscles.

EZH2 expression in proliferating satellites

Because deflazacort mainly exerts its beneficial effects in muscle through immune modulation, we sought to identify a distinct pathway that can provide additional, complementary benefit in DMD treatment. First, we examined variations in gene expression across

the trajectory of muscle differentiation from satellite cells to myocytes among control, BMD, and DMD muscles. Figure 3A focuses on the muscle structure development and muscle cell differentiation pathways that were specifically up-regulated in controls compared to BMD and DMD muscles.

The results of this analysis led us to focus on satellite cells as they are the source of myocytes (*36*, *37*) and proliferate in response to a various kinds of muscle damages (*38*–*40*). First, we assigned each cell type a quantitative score for cell proliferation based on expression of G_2-M and S phase markers (Materials and Methods; Fig. 3, B and C). Notably, satellite cells included a group of actively proliferative cells within samples originating from both patients with BMD (3.01%; Fisher's exact test $P = 2.1 \times 10^{-6}$) and patients with DMD (5.21%; Fisher's exact test $P = 5.2 \times 10^{-16}$), demonstrating elevation of proliferative activity in compensation for damaged muscle tissues. This observation was specific to satellite cells (Fig. 3B and fig. S8). Similar scoring of cell types was performed for markers of apoptotic and necrotic cell death but found no substantial differences between healthy and patient cells (fig. S8).

Next, we examined genes showing differential expression profiles in proliferating satellite cells across control, BMD, and DMD muscles (Fig. 3D). Among these, *EZH2* stood out for being known to play a key

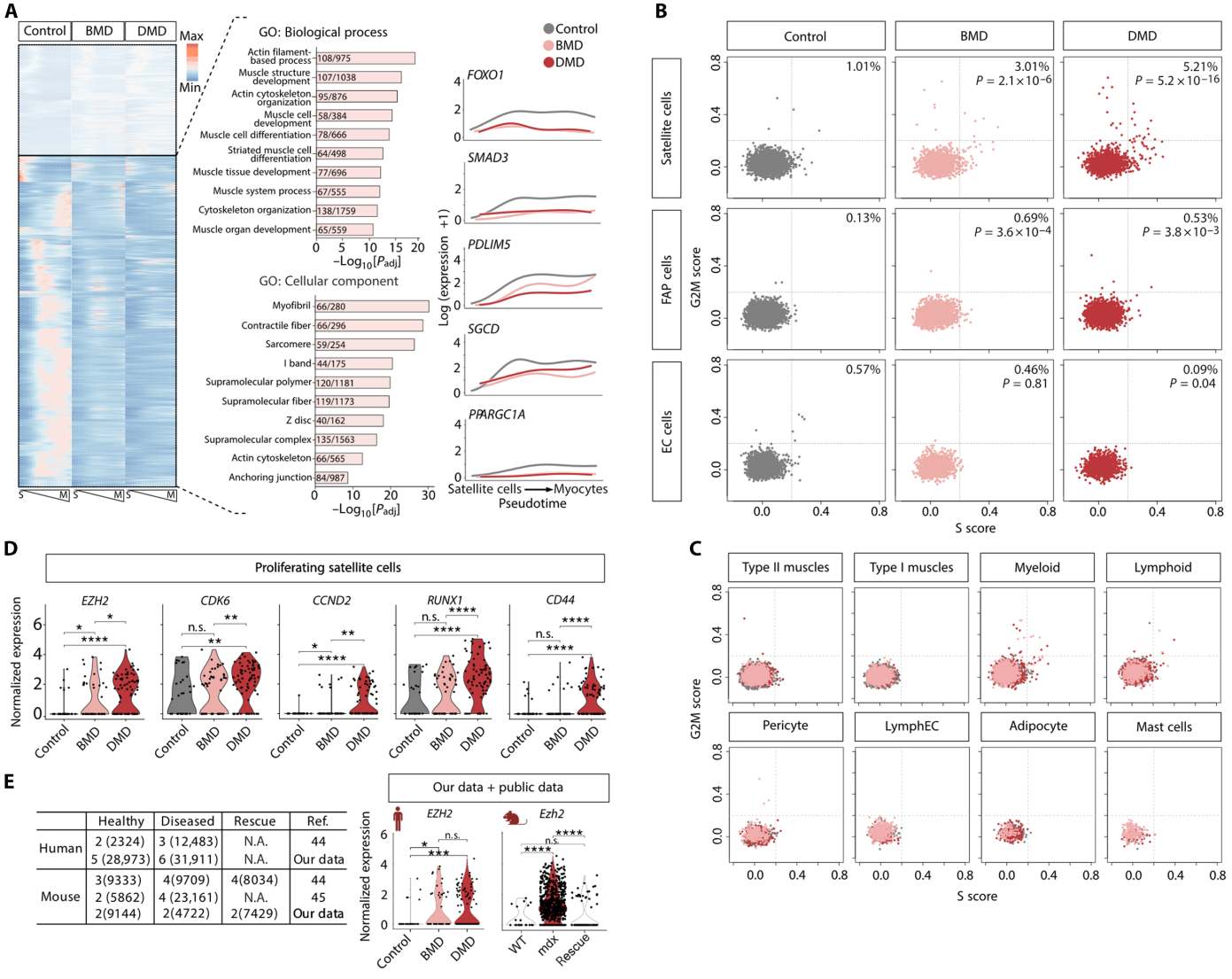

Fig. 3. Proliferating satellite cells in patients with DMD lead to increased signal transduction in a pathway involving *EZH2* and cell cycle progressors. (**A**) Heatmap of genes whose expressions vary over pseudo-temporal ordering from satellite cells (S) to myocytes (M) (left). Gene ontology (GO) terms enriched among these genes (middle). Numbers in bar graphs indicate numbers of input genes/genes in annotation. Plots of log-transformed counts and the fitted values of control, BMD, and DMD patient cells (right). (**B** and **C**) Scatterplots of cell cycle scores in all cell types by disease status. Cells in different disease groups are plotted separately in (B) but plotted together in (C). (B) Satellite cells, FAP cells, and EC cells. (C) Type II muscles, Type I muscles, Myeloid, Lymphoid, Pericyte, LymphEC, Adipocyte, and Mast cells. Control samples are shown in gray, BMD samples are shown in pink, and DMD samples are represented in red. Cells were considered positive for cell proliferation if they harbor positive scores for either G2M or S. (**D**) Violin plots depicting DEGs in proliferating satellite cells. (**E**) Table displaying the number of samples and corresponding cell counts (in parentheses) included in our and previous studies (left). Violin plots of both human *EZH2* and mouse *Ezh2* expression in our and public data. n.s. denotes *P* value > 0.05; $*P \leq 0.05$; $**P \leq 0.01$; $***P \leq 0.001$; $****P \leq 0.0001$. N.A., not applicable.

role in regulating gene expression in muscle cells (*22*, *41*) and for drugs targeting its gene products being actively used for cancers (*42*, *43*). The differential expression of *EZH2* in both patients with DMD and D2-mdx mice was corroborated through data integration with publicly available datasets (Fig. 3E) (*44*, *45*). Therefore, proliferating satellite cells mark increased activity of a signal transduction pathway that engages EZH2 and proteins associated with cell cycle progression in the cells of patients with muscular dystrophy.

Improvement of muscle phenotype through EZH2 inhibitor administration in mice

Down-regulation of *Ezh2* is known to cause muscle gene activation and myoblast differentiation (*46*), whereas its increased expression inhibits muscle differentiation in vitro (*22*). Therefore, we sought to test whether administration of an EZH2 inhibitor elicits an improvement in muscle phenotype in DMD through increased muscle cell differentiation. EZH2 inhibitors, GSK126 and tazemetostat, were administrated with or without deflazacort to D2-mdx mice (Fig. 4A). Representative hematoxylin and eosin (H&E) staining images representing each treatment group's quadriceps muscles are presented in Fig. 4B; this staining revealed features characteristic of dystrophinopathy. In particular, D2-mdx mice treated with EZH2 inhibitors exhibited improvement in dystrophinopathy in comparison to vehicle-treated mutant mice, in a degree similar or better compared to deflazacort-treated mice (Fig. 4, C to E, and fig. S9). When relative areas of collagen were compared (Materials and Methods), D2-mdx mice treated with EZH2 inhibitors exhibited improvement in dystrophinopathy in comparison to vehicle-treated mutant mice, in a degree similar to deflazacort-treated mice (Fig. 4E). The percentage of centrally located nuclei was highest in untreated D2-mdx samples and showed the greatest reduction in D2-mdx samples treated with deflazacort and tazemetostat (Fig. 4F). Furthermore, cross-sectional areas of muscle fibers were smallest in untreated D2-mdx samples and largest in those treated with deflazacort and tazemetostat (Fig. 4G). Last, grip strength was substantially increased in mice given tazemetostat with or without deflazacort compared to deflazacort-only mice (Fig. 4H).

Compensation of deflazacort's negative effects through EZH2 inhibition in D2-mdx mice

To understand the potential consequences of EZH2 inhibition, we performed snRNA-seq on muscle samples from mice given various drug treatments. Following quality control measures, a total of 37,464 nuclei were retained for subsequent analyses (Fig. 5A). Distinct patterns emerged within the cellular landscape, wherein myeloid and lymphoid lineage cells displayed the most pronounced expansion in untreated D2-mdx mice, whereas muscle cells exhibited expansion in D2-mdx mice given GSK126 (Fig. 5B). Cell cycle scoring of myeloid lineage cells revealed a notable variance, with untreated D2-mdx mice manifesting the highest proliferative status ($P < 2.2 \times 10^{-16}$; Fig. 5C). Differential expression analyses of cytokine- and inflammation-related genes uncovered up-regulation in untreated D2-mdx mice compared to counterparts administered deflazacort and/or GSK126 (Fig. 5D). In particular, the profibrotic genes in FAP cells illustrated in Fig. 2H were down-regulated in mice that received GSK126 (Fig. 5E).

Next, we focused on the beneficial effect of EZH2 inhibition on the myocyte differentiation process. Leveraging single-cell regulatory network inference and clustering analyses, we observed D2-mdx mice treated with GSK126 showing activation of *Myog*, a transcription factor pivotal to muscle differentiation, within satellite cells (Fig. 6, A and B). In contrast, untreated counterparts did not show *Myog* activation (fig. S10). Figure 6C presents the computed t-distributed stochastic neighbor embedding (t-SNE) visualization of all cells based on the *Pax7* (a pan-satellite cell marker) and *Myog* activity in D2-mdx mice given GSK126. Genes associated with muscle structural elements, illustrated in Fig. 2G, also demonstrated elevated expression in D2-mdx mice treated with GSK126, signifying a potential beneficial effect on muscle architecture (Fig. 6D). To explain this unexpected effect, we queried EZH2-binding sites in muscle cells using ENCODE project data. This revealed a group of genes that were both differentially expressed in proliferating satellite cells and bound by EZH2 to be enriched for cell polarity-related genes (Fig. 6, E and F), suggesting a possible restoration of muscle stem cell polarity due to EZH2 inhibition. Binding sites for EZH2 were identified near the *JAM3* locus, one of the genes that were differentially expressed in patients' proliferating satellite cells and were bound by EZH2 (Fig. 6F). A heatmap of the differentiation trajectory analysis revealed disrupted signatures in D2-mdx mice, specifically an overall increase in cell cycle and proliferation markers (Fig. 6G). However, following administration of deflazacort and GSK126, the gene expression pattern resembled that of the wild type. The same pattern persists when GSK126 is given alone (fig. S11).

DISCUSSION

DMD is both the most prevalent and the most severe form of muscular dystrophy, typically resulting in a life expectancy limited to the early 20s (*47*, *48*). Steroids still remain as the standard of care despite known side effects such as obesity and osteopenia (*18*); development of additional treatments thus remains imperative. Using snRNA-seq to capture the transcriptomes of individual muscle cells from human patients and model mice, we have uncovered a notable expansion of *EZH2* expression within proliferating satellite cells. Furthermore, we have demonstrated that inhibition of EZH2 has the potential to mitigate immune signals and ameliorate the phenotypic manifestations of DMD.

A few recent studies have examined the pathophysiology of DMD muscles at the single-cell level, including one that analyzed skeletal muscle cellular diversity in human patients and D2-mdx mice with and without exon skipping therapy (*44*). Another study observed increased expression of FAP cells, consistent with our findings, and up-regulation of plasminogen activator inhibitor-1 (*PAI1*) in dystrophic endothelial cells (*45*). In the skeletal muscle of mice with *DMD* exon 51 deletion, another study identified distinctive myonuclear subtypes within dystrophin myofibers and explored transcriptional pathways associated with degeneration and regeneration in DMD (*49*). Consistent with the previous reports, we observed both patients with DMD and D2-mdx mice displaying reduced myocytes and increased immune cells, which imbalance was partly reverted in mice by the administration of deflazacort. The profiles of BMD muscle were closer to normal than those of DMD (Fig. 1D), reflecting the milder symptoms of patients with BMD. It would be of interest to further investigate the genetic and phenotypic correlation of *DMD* mutations and disease severity (*50*). Our study uncovered a colocalization of satellite cells and immune cells in the inflamed muscle tissue of patients with DMD (Fig. 1, I and J, and fig. S12). This close proximity of satellite cells and immune cells may possibly account for the increased expression of *EZH2* and increased inflammation observed in patients with

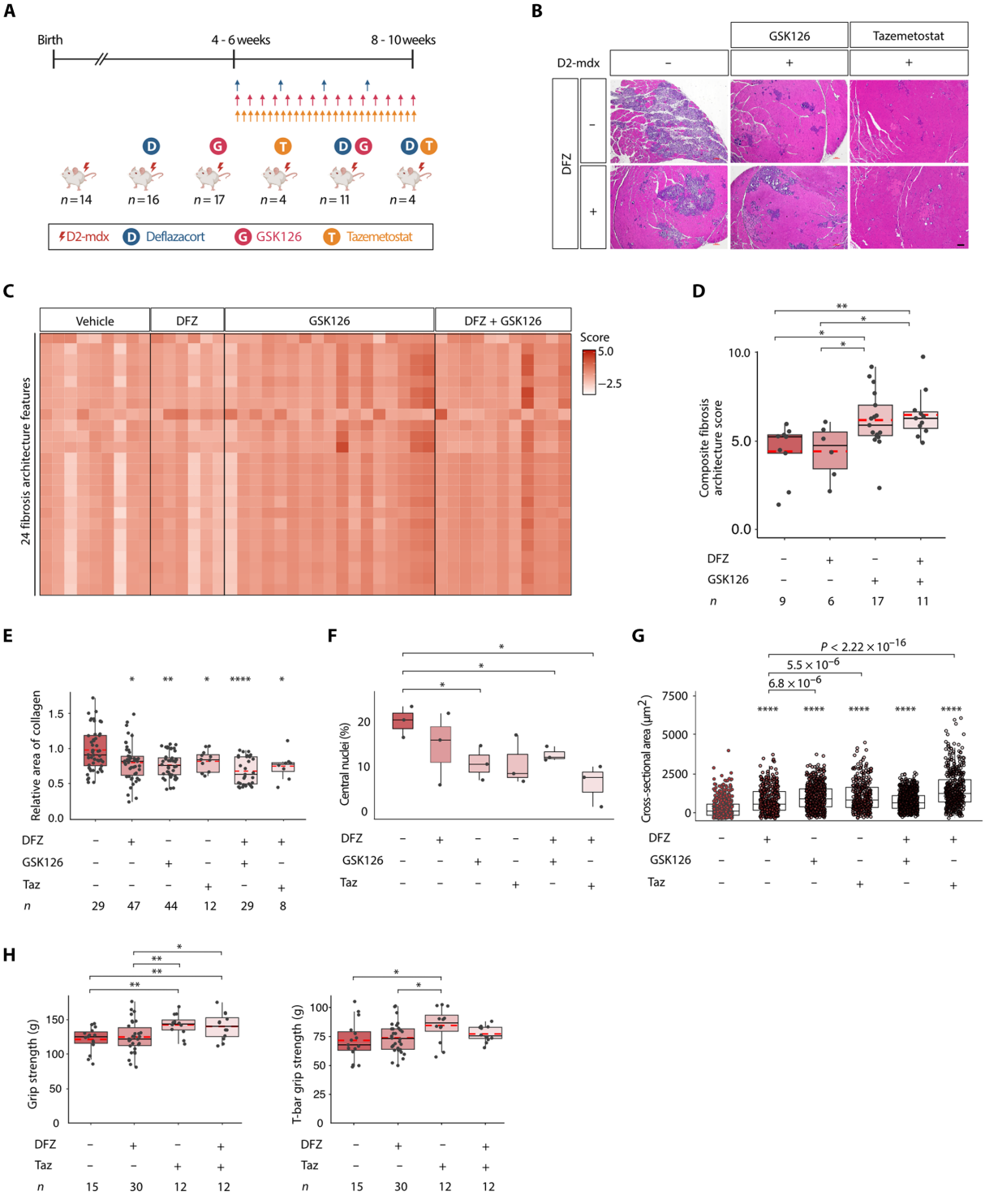

Fig. 4. Treatment with EZH2 inhibitors improved muscle phenotype in D2-mdx mice. (**A**) Schematic representation of the experimental setup involving mouse drug administration. (**B**) H&E staining of muscle tissues from the 8- to 10-week-old mice after injection of deflazacort and/or GSK126 and/or tazemetostat (Taz). Scale bar, 100 μm. (**C**) Heatmap showing the quantification of Masson's trichrome images for fibrosis architecture features from mice with or without GSK126 treatment. Feature names (row) are listed separately in data S2. (**D**) Composite fibrosis scores calculated on the basis of (C). The number indicates the number of mice used. (**E**) Boxplot showing the quantification of area of collagen relative to untreated D2-mdx in mice with or without drug treatment based on Masson's trichrome–stained images. The number indicates the number of slides used. (**F**) Boxplot showing the percentage of central nuclei in muscle fibers. (**G**) Boxplot showing cross-sectional areas of muscle fibers. Asterisks without brackets are the comparison with the control. (**H**) Boxplots showing grip strength (left) and T-bar grip strength (right) of 8- to 10-week-old mice after injection of deflazacort and/or tazemetostat. Red dotted lines indicate the mean. The number represents the triplication of the initial count of mice used. *$P \leq 0.05$; **$P \leq 0.01$; ****$P \leq 0.0001$.

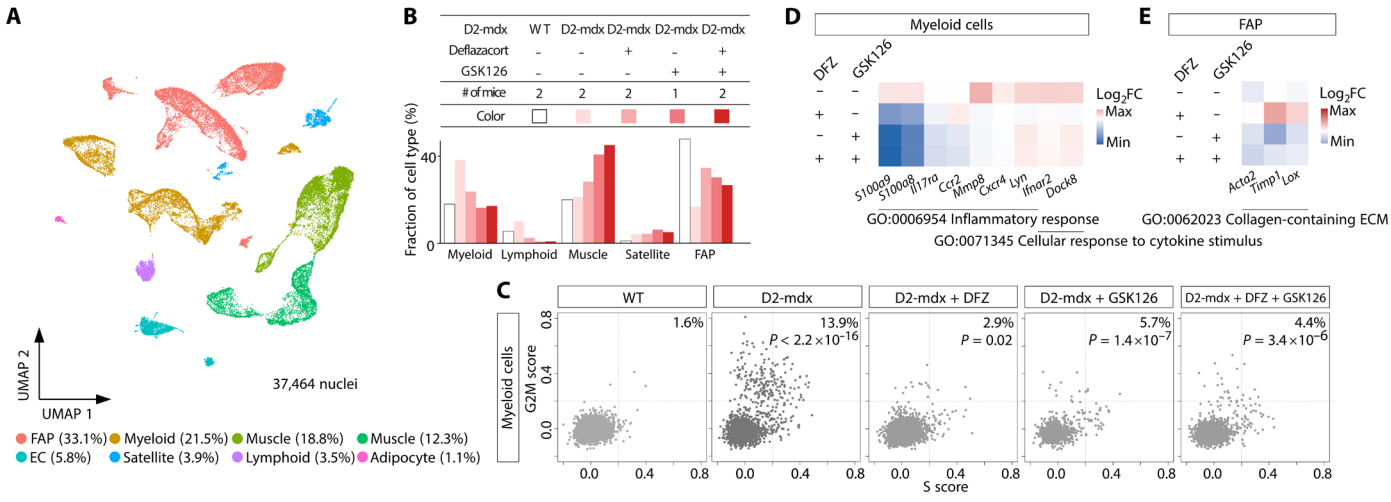

Fig. 5. EZH2 inhibitor maintains the immune suppressing effect and overrides the increased fibrosis induced by deflazacort. (**A**) UMAP visualization of 37,464 nuclei from muscle tissues of wild-type or D2-mdx mice with drug treatments. (**B**) Cell type proportion by treatment status. (**C**) Scatterplots of cell cycle scores in myeloid cells by treatment status. (**D**) Heatmap of the DEGs in myeloid cells by treatment status. (**E**) Heatmap of the DEGs in FAP cells shown in Fig. 2H by treatment status.

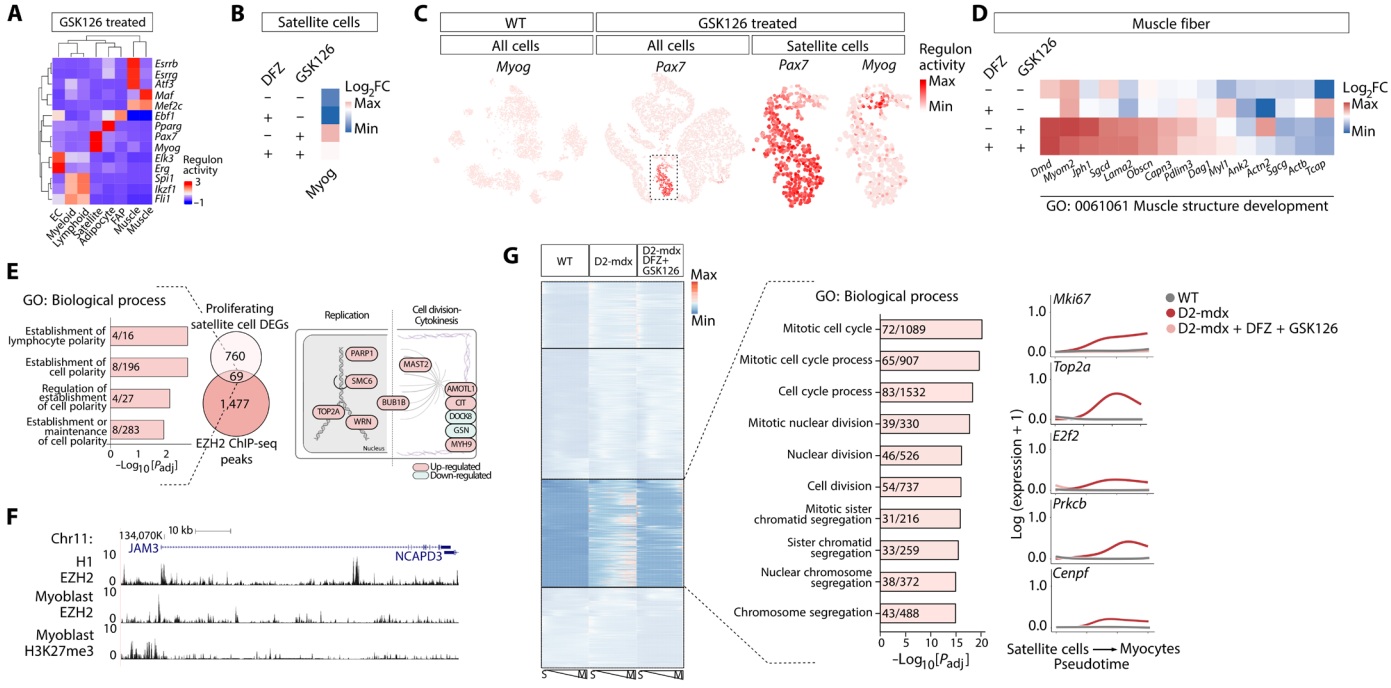

Fig. 6. EZH2 inhibitor overrides the muscle weakness effect exerted by deflazacort through stimulating muscle differentiation. (**A**) Heatmap of differentially enriched regulators for each cell type in GSK126-injected mice. (**B**) Heatmap of *Myog* expression in satellite cells by treatment status. (**C**) t-SNE visualization of *Pax7* and *Myog* transcription factor activities in cells of wild-type and GSK126-injected mice. (**D**) Heatmap of the muscle cell DEGs shown in Fig. 2G by treatment status. (**E**) Number of genes differentially expressed in the proliferating satellite cells and bound by EZH2 (left). Numbers in bar graphs indicate numbers of input genes/genes in annotation. Schematic representation of the roles of overlapping genes that are engaged in cell polarity group (right). (**F**) Diagram of the exemplary EZH2 ChIP-seq peak locus on *JAM3*, a DEG found in the proliferating satellite cells and bound by EZH2. (**G**) Heatmap of genes whose expression varies over pseudotemporal ordering from satellite cells to the differentiated myocyte state (left). Numbers in bar graphs indicate input genes/genes in annotation. Plots of log-transformed counts and the fitted values of wild-type mice, D2-mdx mice, and D2-mdx mice with deflazacort and GSK126 injection (right).

DMD. Although steroids are commonly used in the clinic, the particular molecular cascades they alter have remained elusive. In this study, we found that deflazacort treatment reduced actin remodeling and inflammatory signals in immune cells through NR3C1 binding elements, suggesting a possible mode of action of steroids in DMD treatment (Fig. 2).

Previous studies have observed cellular consequences of reduced EZH2 function in various biological contexts. In cancers, *EZH2* knockdown induces cell cycle arrest and impairs in vitro migration and invasion (*51*–*53*), whereas depletion of *Ezh2* results in diminished activation of macrophages and microglia (*54*). Here, we further demonstrated molecular mechanisms underlying the immunosuppressive effects of Ezh2 inhibition. Inflammatory monocyte-derived macrophages were known to play a critical role in DMD pathogenesis, and CCR2 deficiency helped restore the macrophage polarization balance by preventing an excessive shift toward a proinflammatory phenotype (*55*). *CCR2* was decreased with EZH2 inhibitor treatment (Fig. 5D), suggesting that CCR2 could potentially be targeted therapeutically with EZH2 inhibitor.

Through genome-wide mapping of histone modifications in muscle satellite cells and studying mice lacking *Ezh2* in satellite cells, it was found that Ezh2 activity is required for satellite cell proliferation (*56*). In the context of DMD, *EZH2* appears to be a double-edged sword. On one hand, the increased presence of EZH2 in satellite cells could be beneficial, potentially serving as a compensatory mechanism to counteract the detrimental effects of DMD through supporting satellite cell proliferation. However, inhibiting EZH2 may encourage satellite cells to differentiate and contribute to muscle repair. Striking the right balance between promoting proliferation and differentiation of satellite cells may optimize therapeutic strategies for patients with DMD. A previous study demonstrated that satellite cell-specific ablation of *Ezh2* in mice resulted in reduced muscle mass and impaired regeneration (*41*). This experimental outcome reflects different experimental conditions, with ours being based on pharmacological inhibition in mature muscle. Nevertheless, the study also observed increased expression of myogenic and satellite cell-specific expression, consistent with our findings (*41*). Here, we elucidated the precise role of EZH2 and its implications in DMD treatment. The augmented expression of EZH2 in proliferating satellite cells supports a state of active proliferation and hence hindered muscle differentiation (Fig. 3) (*22*). Administration of EZH2 inhibitors in D2-mdx mice reduced fibrosis (Fig. 4). These findings underscore the potential contribution of EZH2 inhibitors to the attenuation of adipogenic or fibrotic regions (Fig. 5E). Furthermore, we observed GSK126 administration increasing the expression of genes associated with muscle organization through forming a sequence of differentiating lineages, progressing from $Pax7^{+}Myog^{-}$, $Pax7^{+}Myog^{+}$, and ultimately to the $Pax7^{-}Myog^{+}$ fetal myocytes-like lineage (Fig. 6, A to C, and fig. S13) (*57*), and possible restoration of satellite cell polarity. JAM3, one of the genes that are differentially expressed in patients' proliferating satellite cells and were bound by EZH2, is a cell adhesion molecule that is primarily localized at cell junctions, where it regulates intercellular communication and maintains the integrity of cellular barriers (*58*). In muscle stem cells, JAM3 may play a role in maintaining proper cell divisions, especially during muscle regeneration and repair processes (Fig. 6F) (*59*). The beneficial effect was not only found in satellite cells but also in other cell types.

A recent study demonstrated a nontranscriptional pathway that steroid can incur anti-inflammatory effects by reshaping the mitochondrial metabolism of macrophages, leading to increased tricarboxylic acid (TCA) cycle activity and subsequent itaconate synthesis (*60*). Increased TCA cycle activity was also observed in our data from mice treated with deflazacort alone but reverted by the EZH2 inhibitor (fig. S14). One could postulate that the inhibition of EZH2 overrides the up-regulation of the TCA cycle through altering mitochondrial function as it is a prominent characteristic of DMD (*1*, *49*). However, we did not observe notable changes in the expression of genes associated with mitochondrial metabolism in both mouse muscle fiber and myeloid clusters (fig. S15).

Although our findings suggest EZH2 inhibition as a promising therapeutic option that can be used in conjunction with deflazacort, more detailed molecular mechanisms are still needed. The ChIP-seq analysis of proliferating satellite cells might offer insights into the direct targets of EZH2 inhibition. However, such an experiment cannot presently be performed owing to the paucity of human proliferating satellite cells. We anticipate that the advent of new methodologies that require less sample input will help to elucidate these direct targets. In addition to that methodological limitation, it is notable that myofibers in DMD are known to undergo necrotic and apoptotic processes (*61*, *62*); however, none of the these signatures were detected in our analysis (fig. S8). Presumably, the cells harboring these signatures were filtered out during the quality control step. We aimed to use two different species assuming their conserved response to *DMD* mutation. However, there appears to be a noticeable discrepancy in the effect on lymphoid cells (Fig. 2D). Specifically, despite the parallel responses observed in myeloid cells (Fig. 2A), human lymphoid cells exhibited a lesser degree of susceptibility compared to their mouse counterparts.

Although we demonstrate that EZH2 inhibitors have therapeutic potential, particularly for muscle-related diseases, the long-term consequences on satellite cell dynamics and potential off-target effects must be carefully considered. Future studies are needed to investigate the dose-dependent and temporal effects of EZH2 inhibition to balance the therapeutic benefits against possible adverse outcomes, especially in nonmuscle tissues.

Collectively, our comparative analysis of human patients and a mouse DMD model have unveiled genes and pathways that exhibit selective down-regulation in immune cells and concurrent up-regulation in muscle organizational cells. This finding suggests a potential therapeutic target with promising implications for the treatment of DMD.

MATERIALS AND METHODS

Human participants

Muscle biopsies from patients were performed in accordance with informed written consent from the Seoul National Hospital Children's Hospital institutional review board–approved protocols (no. 1009-030-331). The patients did not take any medication at the time of the biopsy. Muscle samples were taken from the quadriceps femoris and frozen with isopentane cooled in liquid nitrogen as described previously (*63*). Healthy muscle samples were acquired from the quadriceps or abdomen of subjects undergoing surgery for nonmuscular symptoms. snRNA-seq was performed on fresh frozen quadriceps femoris obtained from three male individuals with DMD, three male individuals with BMD, and five healthy control individuals (Materials and Methods; Fig. 1A, fig. S1, and table S1). Among the control samples, three were derived from abdominal muscle tissue undergoing surgery for nonmuscular symptoms. All participants were under the age of 17, and each group was composed of individuals of similar ages.

Mouse strains

DBA/2J and DBA/2J-mdx mice (D2.B10-*Dmd*^{mdx}/J), hereafter denoted as D2-mdx mice, were purchased from the Jackson Laboratory (JAX ID: 013141; Bar Harbor, ME). All experiments were approved by the Institutional Animal Care and Use Committee in Seoul National University Hospital (no. 20-0216-S1A0), and animals were maintained in a facility accredited by Association for Assessment and Accreditation of Laboratory Animal Care (AAALAC) International (no. 001169) in accordance with the Guide for the Care and Use of Laboratory Animals (eighth edition, National Research Council). Muscle samples were taken from the hindlimb and quadriceps and frozen with liquid nitrogen. snRNA-seq was performed on fresh frozen muscle cells from two male wild-type DBA/2J mice, two male D2-mdx mice, and two male D2-mdx mice treated with deflazacort. Each genotype group included one 7-week-old and one 28-week-old mouse.

Generating and processing snRNA-seq data

All muscle samples were processed and snRNA-seq data generated by GENINUS (Seoul, Republic of Korea). After the frozen tissue was homogenized and nuclei were counted, the nuclei were isolated using flow cytometry. Single-cell capture, barcoding, and library preparation were performed following the 10x Genomics Single cell Chromium 3′ protocols (V3: CG000183). cDNA library quality was determined using an Agilent Bioanalyzer. Paired-end 200–base pair (bp) reads were generated on an Illumina NovaSeq5000/6000.

Analysis of snRNA-seq data

Generated FASTQ files were mapped to either human (GRCh38/hg38 pre-mRNA genome) or mouse (mm10) transcriptome references provided by 10x Genomics using Cell Ranger v6.0.0. The output was processed using Seurat v4.0.1 (*64*). We then applied standard cell filtering criteria (nFeature_RNA > 200, nFeature_RNA < 5000, and percent.mt < 5). Nuclei that passed the filtering were normalized and integrated with LIGER v1.0.0 (*65*).

Genes that were differentially expressed between patient and control tissues were defined in each cluster using the FindMarker function of Seurat. SCENIC v1.3.1 was used to infer transcription factor–target relationships (*66*). CellChat was used to infer intercellular communications (*67*). Slingshot was used for cell lineage and pseudotime inference (*68*). TradeSeq was used for trajectory-based differential expression analysis (*69*). Gene set enrichment analysis was performed using the escape R package, v1.99.0 (*70*). For mouse immune subclustering analysis, data from the Single-Cell Muscle Project were used (*71*–*74*). NicheNet was used for predicting ligand and target gene interactions (*75*).

Analysis of public snRNA-seq data

Data from Scripture-Adams *et al.* (*44*) and Saleh *et al.* (*45*) were obtained from the National Center for Biotechnology Information (NCBI) Gene Expression Omnibus (GEO) (GSE213925) and Sequence Read Archive (SRA) (PRJNA976807). These data were reanalyzed following the same procedures used for our data as described in the "Analysis of snRNA-seq data" section. Statistical analyses were performed using a *t* test to compare between groups.

Chromatin immunoprecipitation sequencing

RAW264.7 cells (Korean Cell Line Bank, KLCB 40071) were cultured and treated with deflazacort (10^{-6} M) for 24 hours. The cells were harvested and treated with 2 mM disuccinimidyl glutarate (DSG) for 35 min, followed by incubation with 1% formaldehyde for 10 min for double fixation. To quench the fixation, 125 mM glycine was added. The cells were then permeabilized, and the cell pellet was resuspended in 1% SDS lysis buffer [50 mM tris-HCl (pH 8), 10 mM EDTA, 1% SDS, and protease inhibitor]. Sonication was performed (Covaris S220, power: 175 W; duty factor: 10%, cycles per burst: 200, and 430 s), and the solution was diluted 10-fold with dilution buffer [16.7 mM tris-HCl (pH 8), 0.01% SDS, 1% Triton X-100, 167 mM NaCl, 1.2 mM EDTA, and protease inhibitor]. After centrifugation (13,000 rpm, 15 min, 4°C), the supernatant was incubated with antibody-conjugated beads (Invitrogen, 10003D) on a rotator (25 rpm, 4°C, overnight). The beads used were preincubated with Nr3c1 antibodies (Santa Cruz Biotech, sc-293232) for 4 hours prior to mixing with the sample (rotator 25 rpm, 4°C). Following immunoprecipitation, a washing step was performed, and RNase A was added and shaken (Thermomixer, 400 rpm, 37°C, 30 min). SDS and proteinase K were added, and incubation was carried out to elute the fragment DNA (Thermomixer, 200 rpm, 65°C, overnight). Size selection was performed to isolate eluted fragments between 200 and 300 bp (Beckman, A63881). The fragmented DNA was then end repaired, dA tailed, and ligated to the sequencing adapters (NEB, E7645). One nanogram of the ligated fragments was amplified through 10 cycles of polymerase chain reaction, and paired-end sequencing was conducted on the resulting library. ChIP-seq data processing and analysis were performed using the nf-core/chipseq pipeline (*76*).

Gene set enrichment analysis

Cell cycle scores were assigned using the CellCycleScoring() function in Seurat. Scoring was based on the strategy described by Tirosh *et al.* (*77*), and the full gene list is in data S3. We called cells "proliferating" if S.Score or G2M.Score were > 0.2. Gene set enrichment analysis was performed using the escape R package v1.99.0 (*70*). Gene sets were derived from the Molecular Signature Database (https://gsea-msigdb.org/gsea/msigdb/).

Generation, processing, and analysis of spatial transcriptomics data

Samples processing and data generation using the Visium platform was done by GENINUS. Experiments were performed using the Visium Spatial Platform 3′ v1 (PN-1000193, PN-1000184, and PN-1000215). Sequencing reads from Visium ST (10x Genomics) experiments were first preprocessed with Space Ranger v1.3.1 and mapped to the human reference genome (GRCh38). The count matrices were subsequently analyzed using cell2location v0.1.3 (*78*). To discriminate transcriptionally distinct cell populations with MERFISH, we designed a panel of 300 genes selected based on cluster markers identified from snRNA-seq data.

ChIP-seq data analysis

ChIP-seq data for NR3C1 (A549 cells: ENCFF638NRS), H3K4me1 (A549 cells: ENCFF040HPO), H3K27ac (A549 cells: ENCFF541LPH), EZH2 (myoblast: ENCFF353VYD; H1 cells: ENCFF109KCQ), and H3K27me3 (myoblast: ENCFF261INX) in the bigwig format were downloaded from the ENCODE project (https://encodeproject.org/) and visualized in the UCSC Genome Browser (*79*). ChIPseeker (*80*, *81*) was used to annotate ChIP peaks.

Drug treatment

Deflazacort (SML0123-10MG; Sigma-Aldrich, St. Louis, MO) was formulated as a suspension (0.2 mg/ml) in a solution composed of

dimethyl sulfoxide (DMSO) (10%), polyethylene glycol, molecular weight 300 (PEG-300) (40%), Tween 80 (5%), and saline (45%). This formulation was administered at a dose of 1 mg/kg by intraperitoneal injection once a week for 28 days to 4-week-old mice. GSK126 (S7061; Selleck Chemicals, Houston, TX) was administered to 4-week-old mice by intraperitoneal injection once every 2 days for 28 days at a dose of 50 mg/kg in 20% Captisol (*43*, *82*). Tazemetostat (S7128; Selleck Chemicals, Houston, TX) (400 mg/kg, 0.5% CMC-Na and 0.1% Tween 80 in water) was orally administrated daily for 28 days (*83*, *84*). For the deflazacort untreated group, the vehicle consisted of DMSO (10%), PEG-300 (40%), Tween 80 (5%), and saline (45%) (*85*). For the GSK126 control group, 20% Captisol was used as the vehicle (*82*). The vehicle for the tazemetostat control group was composed of 0.5% CMC-Na and 0.1% Tween 80 in water (*83*). The 14 untreated control mice, as shown in Fig. 4A, are a combination of different vehicle-treated animals (three deflazacort vehicle-treated, six deflazacort and GSK126 combined vehicle-treated, and five deflazacort and tazemetostat combined vehicle-treated). D2-mdx mice aged 4 to 6 weeks were examined. Fourteen untreated D2-mdx mice were used as controls. The treatment groups included 16 mice given deflazacort, 17 given GSK126, and 4 given tazemetostat. Eleven mice were treated with both deflazacort and GSK126, and 4 mice were treated with both deflazacort and tazemetostat.

Histology and image quantification

After embedding fixed tissues in paraffin, 4-μm sections were stained with Masson's trichrome stain using the Biognost Masson Trichrome kit (MST-K-500) according to the manufacturer's protocol and imaged at 40x using a ZEISS Axioscan 7 (ZEISS, Germany). To quantify areas of collagen, we prepared slides so that each slide contains a cross section covering the entire quadriceps. Then, Python's PIL Image and ImageDraw modules were used to automate the quantification of tissue and collagen regions in Masson's trichrome histological images. Samples were triplicated. Images were segmented using thresholds and quantified through pixel counting.

For FibroNest (PharmaNest, Princeton, NJ) analysis, the images were cleaned and processed for anomalies such as scanning stripes, image compression artifacts, rinsing artifacts, dusts, and saturated pixels. The digital images were then processed and segmented to allocate the collagen biological marker to a specific channel as FibroNest selects a region of interest based on collagen fibers. These analyses were blinded to clinical and histological data.

To count the ratio of cells with central nuclei, such cells were manually annotated by identifying nuclei positions within each muscle fiber. To calculate muscle fiber sizes, Cellpose3 (*86*) was used to segment cells in the histology slides, and the mask output was used to measure the cross-sectional areas with scikit-image's regionprops function. Both analyses were performed on the same region of the quadrecep muscles.

Behavioral tests

The behavioral assessment was conducted 1 day prior to tissue collection. Mice were moved to the behavioral assessment room 30 min before the test to allow them to acclimate to the new environment. For T-bar grip strength test, the forepaws were stably positioned on the T-bar, and the mouse was pulled gently backward to measure the strength of the forelimb. For grip strength test, the grid was attached securely to the sensor. Both its forepaws and hindpaws were stably positioned. The mouse gently pulled backward, and while sliding down, the force with which it grips the wire was measured. The tests were repeated three times. The calculations for grip strength were adapted from Long *et al.* (*87*) and Laurila *et al.* (*88*). Behavioral tests were performed in a blinded manner.

Statistical analysis

For statistical analysis, R version 4 was used. Statistical analyses for single-cell genomics experiments are described in the preceding subsections. Statistical comparisons between groups were assessed with Fisher's exact test (Fig. 3B) or *t* tests. A P value of ≤ 0.05 was considered statistically significant.

Supplementary Materials

The PDF file includes:

Figs. S1 to S15
Tables S1 to S4
Legends for data S1 to S3

Other Supplementary Material for this manuscript includes the following:

Data S1 to S3

REFERENCES AND NOTES

1. D. Duan, N. Goemans, S. i. Takeda, E. Mercuri, A. Aartsma-Rus, Duchenne muscular dystrophy. *Nat. Rev. Dis. Primers.* **7**, 13 (2021).
2. J. K. Mah, L. Korngut, J. Dykeman, L. Day, T. Pringsheim, N. Jette, A systematic review and meta-analysis on the epidemiology of Duchenne and Becker muscular dystrophy. *Neuromuscul. Disord.* **24**, 482–491 (2014).
3. S. M. Hoy, Delandistrogene moxeparvovec: First approval. *Drugs* **83**, 1323–1329 (2023).
4. FDA, FDA Approves First Gene Therapy for Treatment of Certain Patients with Duchenne Muscular Dystrophy (FDA, 2023); https://fda.gov/news-events/press-announcements/fda-approves-first-gene-therapy-treatment-certain-patients-duchenne-muscular-dystrophy.
5. A. Lek, B. Wong, A. Keeler, M. Blackwood, K. Ma, S. Huang, K. Sylvia, A. R. Batista, R. Artinian, D. Kokoski, S. Parajuli, J. Putra, C. K. Carreon, H. Lidov, K. Woodman, S. Pajusalu, J. M. Spinazzola, T. Gallagher, J. LaRovere, D. Balderson, L. Black, K. Sutton, R. Horgan, M. Lek, T. Flotte, Death after high-dose rAAV9 gene therapy in a patient with Duchenne's muscular dystrophy. *N. Engl. J. Med.* **389**, 1203–1210 (2023).
6. N. Elangkovan, G. Dickson, Gene therapy for Duchenne muscular dystrophy. *J. Neuromuscul. Dis.* **8**, S303–S316 (2021).
7. E. Erkut, T. Yokota, CRISPR therapeutics for Duchenne muscular dystrophy. *Int. J. Mol. Sci.* **23**, 1832 (2022).
8. S. Kim, K. A. Campbell, D. J. Fox, D. J. Matthews, R. Valdez, MD STARnet, Corticosteroid treatments in males with Duchenne muscular dystrophy: Treatment duration and time to loss of ambulation. *J. Child Neurol.* **30**, 1275–1280 (2015).
9. S. Kourakis, C. A. Timpani, D. G. Campelj, P. Hafner, N. Gueven, D. Fischer, E. Rybalka, Standard of care versus new-wave corticosteroids in the treatment of Duchenne muscular dystrophy: Can we do better? *Orphanet J. Rare Dis.* **16**, 117 (2021).
10. D. J. Birnkrant, K. Bushby, C. M. Bann, B. A. Alman, S. D. Apkon, A. Blackwell, L. E. Case, L. Cripe, S. Hadjiyannakis, A. K. Olson, D. W. Sheehan, J. Bolen, D. R. Weber, L. M. Ward, DMD Care Considerations Working Group, Diagnosis and management of Duchenne muscular dystrophy, part 2: Respiratory, cardiac, bone health, and orthopaedic management. *Lancet Neurol.* **17**, 347–361 (2018).
11. M. Guglieri, K. Bushby, M. P. McDermott, K. A. Hart, R. Tawil, W. B. Martens, B. E. Herr, E. McColl, C. Speed, J. Wilkinson, J. Kirschner, W. M. King, M. Eagle, M. W. Brown, T. Willis, R. C. Griggs, FOR-DMD Investigators of the Muscle Study Group, V. Straub, H. van Ruiten, A. M. Childs, E. Ciafaloni, P. B. Shieh, S. Spinty, L. Maggi, G. Baranello, R. J. Butterfield, I. A. Horrocks, H. Roper, Z. Alhaswani, K. M. Flanigan, N. L. Kuntz, A. Manzur, B. T. Darras, P. B. Kang, L. Morrison, M. Krzesniak-Swinarska, J. K. Mah, T. E. Mongini, F. Ricci, M. von der Hagen, R. S. Finkel, K. O'Reardon, M. Wicklund, A. Kumar, C. M. McDonald, J. J. Han, N. Joyce, E. K. Henricson, U. Schara-Schmidt, A. Gangfuss, E. Wilichowski, R. J. Barohn, J. M. Statland, C. Campbell, G. Vita, G. L. Vita, J. F. Howard Jr., I. Hughes, H. J. McMillan, E. Pegoraro, L. Bello, W. B. Burnette, M. Thangarajh, T. Chang, Effect of different corticosteroid dosing regimens on clinical outcomes in boys With Duchenne muscular dystrophy: A randomized clinical trial. *JAMA* **327**, 1456–1468 (2022).
12. F. Takeuchi, H. Nakamura, N. Yonemoto, H. Komaki, R. L. Rosales, A. J. Kornberg, A. H. Bretag, C. Dejthevaporn, K. J. Goh, Y.-J. Jong, D.-S. Kim, S. V. Khadilkar, D. Shen, K. T. Wong, J. Chai, S. H.-S. Chan, S. Khan, O. Ohnmar, I. Nishino, S. i. Takeda, I. Nonaka,

Clinical practice with steroid therapy for Duchenne muscular dystrophy: An expert survey in Asia and Oceania. *Brain Dev.* **42**, 277–288 (2020).
13. J. G. Tidball, M. Wehling-Henricks, Evolving therapeutic strategies for Duchenne muscular dystrophy: Targeting downstream events. *Pediatr. Res.* **56**, 831–841 (2004).
14. P. K. Law, T. G. Goodwin, Q. Fang, V. Duggirala, C. Larkin, J. A. Florendo, D. S. Kirby, M. B. Deering, H. J. Li, M. Chen, T. J. Yoo, J. Cornett, L. M. Li, A. Shirzad, T. Quinley, R. L. Holcomb, Feasibility, safety, and efficacy of myoblast transfer therapy on Duchenne muscular dystrophy boys. *Cell Transplant.* **1**, 235–244 (1992).
15. D. De Oliveira Moreira, J. A. Pereira, A. P. Taniguti, C. Y. Matsumura, L. A. Ramos, M. A. Areas, H. S. Neto, M. J. Marques, Suramin attenuates dystrophin-deficient cardiomyopathy in the mdx mouse model of duchenne muscular dystrophy. *Muscle Nerve* **48**, 911–919 (2013).
16. V. Taglietti, K. Kefi, L. Rivera, O. Bergiers, N. Cardone, F. Coulpier, S. Gioftsidi, B. Drayton-Libotte, C. Hou, F.-J. Authier, F. Pietri-Rouxel, M. Robert, D. Bremond-Gignac, C. Bruno, C. Fiorillo, E. Malfatti, P. Lafuste, L. Tiret, F. Relaix, Thyroid-stimulating hormone receptor signaling restores skeletal muscle stem cell regeneration in rats with muscular dystrophy. *Sci. Transl. Med.* **15**, eadd5275 (2023).
17. M. Matsuo, Antisense oligonucleotide-mediated exon-skipping therapies: precision medicine spreading from Duchenne muscular dystrophy. *JMA J.* **4**, 232–240 (2021).
18. H. Wilton-Clark, T. Yokota, Recent trends in antisense therapies for Duchenne muscular dystrophy. *Pharmaceutics* **15**, 778 (2023).
19. C. A. Collins, I. Olsen, P. S. Zammit, L. Heslop, A. Petrie, T. A. Partridge, J. E. Morgan, Stem cell function, self-renewal, and behavioral heterogeneity of cells from the adult muscle satellite cell niche. *Cell* **122**, 289–301 (2005).
20. Y. X. Wang, M. A. Rudnicki, Satellite cells, the engines of muscle repair. *Nat. Rev. Mol. Cell Biol.* **13**, 127–133 (2011).
21. N. C. Chang, F. P. Chevalier, M. A. Rudnicki, Satellite cells in muscular dystrophy—Lost in polarity. *Trends Mol. Med.* **22**, 479–496 (2016).
22. G. Caretti, M. Di Padova, B. Micales, G. E. Lyons, V. Sartorelli, The Polycomb Ezh2 methyltransferase regulates muscle gene expression and skeletal muscle differentiation. *Genes Dev.* **18**, 2627–2638 (2004).
23. W. D. Coley, L. Bogdanik, M. C. Vila, Q. Yu, J. H. Van Der Meulen, S. Rayavarapu, J. S. Novak, M. Nearing, J. L. Quinn, A. Saunders, C. Dolan, W. Andrews, C. Lammert, A. Austin, T. A. Partridge, G. A. Cox, C. Lutz, K. Nagaraju, Effect of genetic background on the dystrophic phenotype in mdx mice. *Hum. Mol. Genet.* **25**, 130–145 (2016).
24. R. M. Keeling, P. T. Golumbek, E. M. Streif, A. M. Connolly, Weekly oral prednisolone improves survival and strength in male mdx mice. *Muscle Nerve* **35**, 43–48 (2007).
25. L. Merlini, A. Cicognani, E. Malaspina, M. Gennari, S. Gnudi, B. Talim, E. Franzoni, Early prednisone treatment in Duchenne muscular dystrophy. *Muscle Nerve* **27**, 222–227 (2003).
26. X. Suárez-Calvet, E. Fernández-Simón, D. Natera, C. Jou, P. Pinol-Jurado, E. Villalobos, C. Ortez, A. Monceau, M. Schiava, A. Codina, J. Verdu-Díaz, J. Clark, Z. Laidler, P. Mehra, R. Gokul-Nath, J. Alonso-Perez, C. Marini-Bettolo, G. Tasca, V. Straub, M. Guglieri, A. Nascimento, J. Diaz-Manera, Decoding the transcriptome of Duchenne muscular dystrophy to the single nuclei level reveals clinical-genetic correlations. *Cell Death Dis.* **14**, 596 (2023).
27. H. Ryu, H. N. Lee, J. Ju, J.-B. Park, E. Oh, M. Z. Lin, J. Seong, Combinatorial effects of RhoA and Cdc42 on the actin cytoskeleton revealed by photoswitchable GEFs. *Sens. Actuators B Chem.* **369**, 132316 (2022).
28. M. Bros, K. Haas, L. Moll, S. Grabbe, RhoA as a key regulator of innate and adaptive immunity. *Cells* **8**, 733 (2019).
29. C. M. Vockley, A. M. D'Ippolito, I. C. McDowell, W. H. Majoros, A. Safi, L. Song, G. E. Crawford, T. E. Reddy, Direct GR binding sites potentiate clusters of TF binding across the human genome. *Cell* **166**, 1269–1281.e19 (2016).
30. S. Gioftsidi, F. Relaix, P. Mourikis, The Notch signaling network in muscle stem cells during development, homeostasis, and disease. *Skeletal Muscle* **12**, 9 (2022).
31. R. Gill, L. Hitchins, F. Fletcher, G. K. Dhoot, Sulf1A and HGF regulate satellite-cell growth. *J. Cell Sci.* **123**, 1873–1883 (2010).
32. C. E. Holterman, F. Le Grand, S. Kuang, P. Seale, M. A. Rudnicki, Megf10 regulates the progression of the satellite cell myogenic program. *J. Cell Biol.* **179**, 911–922 (2007).
33. K. B. Umansky, Y. Gruenbaum-Cohen, M. Tsoory, E. Feldmesser, D. Goldenberg, O. Brenner, Y. Groner, Runx1 transcription factor is required for myoblasts proliferation during muscle regeneration. *PLOS Genet.* **11**, e1005457 (2015).
34. T. Molina, P. Fabre, N. A. Dumont, Fibro-adipogenic progenitors in skeletal muscle homeostasis, regeneration and diseases. *Open Biol.* **11**, 210110 (2021).
35. B. Malecova, S. Gatto, U. Etxaniz, M. Passafaro, A. Cortez, C. Nicoletti, L. Giordani, A. Torcinaro, M. De Bardi, S. Bicciato, F. De Santa, L. Madaro, P. L. Puri, A. Expand, Dynamics of cellular states of fibro-adipogenic progenitors during myogenesis and muscular dystrophy. *Nat. Commun.* **9**, 3670 (2018).
36. Z. Yablonka-Reuveni, The skeletal muscle satellite cell: Still young and fascinating at 50. *J. Histochem. Cytochem.* **59**, 1041–1059 (2011).
37. F. Relaix, M. Bencze, M. J. Borok, A. Der Vartanian, F. Gattazzo, D. Mademtzoglou, S. Perez-Diaz, A. Prola, P. C. Reyes-Fernandez, A. Rotini, V. Taglietti, Perspectives on skeletal muscle stem cells. *Nat. Commun.* **12**, 692 (2021).
38. P. Sousa-Victor, L. Garcia-Prat, P. Munoz-Canoves, Control of satellite cell function in muscle regeneration and its disruption in ageing. *Nat. Rev. Mol. Cell Biol.* **23**, 204–226 (2022).
39. J. E. Morgan, T. A. Partridge, Muscle satellite cells. *Int. J. Biochem. Cell Biol.* **35**, 1151–1156 (2003).
40. N. A. Dumont, C. F. Bentzinger, M.-C. Sincennes, M. A. Rudnicki, Satellite cells and skeletal muscle regeneration. *Compr. Physiol.* **5**, 1027–1059 (2015).
41. A. H. Juan, A. Derfoul, X. Feng, J. G. Ryall, S. Dell'Orso, A. Pasut, H. Zare, J. M. Simone, M. A. Rudnicki, V. Sartorelli, Polycomb EZH2 controls self-renewal and safeguards the transcriptional identity of skeletal muscle stem cells. *Genes Dev.* **25**, 789–794 (2011).
42. K. H. Kim, C. W. Roberts, Targeting EZH2 in cancer. *Nat. Med.* **22**, 128–134 (2016).
43. M. T. McCabe, H. M. Ott, G. Ganji, S. Korenchuk, C. Thompson, G. S. Van Aller, Y. Liu, A. P. Graves, A. Della Pietra III, E. Diaz, L. V. LaFrance, M. Mellinger, C. Duquenne, X. Tian, R. G. Kruger, C. F. McHugh, M. Brandt, W. H. Miller, D. Dhanak, S. K. Verma, P. J. Tummino, C. L. Creasy, EZH2 inhibition as a therapeutic strategy for lymphoma with EZH2-activating mutations. *Nature* **492**, 108–112 (2012).
44. D. D. Scripture-Adams, K. N. Chesmore, F. Barthélémy, R. T. Wang, S. Nieves-Rodriguez, D. W. Wang, E. I. Mokhonova, E. D. Douine, J. Wan, I. Little, L. N. Rabichow, S. F. Nelson, M. C. Miceli, Single nuclei transcriptomics of muscle reveals intra-muscular cell dynamics linked to dystrophin loss and rescue. *Commun. Biol.* **5**, 989 (2022).
45. K. K. Saleh, H. Xi, C. Switzler, E. Skuratovsky, M. A. Romero, P. Chien, D. Gibbs, L. Gane, M. R. Hicks, M. J. Spencer, A. D. Pyle, Single cell sequencing maps skeletal muscle cellular diversity as disease severity increases in dystrophic mouse models. *iScience* **25**, 105415 (2022).
46. I. Marchesi, F. P. Fiorentino, F. Rizzolio, A. Giordano, L. Bagella, The ablation of EZH2 uncovers its crucial role in rhabdomyosarcoma formation. *Cell Cycle* **11**, 3828–3836 (2012).
47. E. Landfeldt, R. Thompson, T. Sejersen, H. J. McMillan, J. Kirschner, H. Lochmüller, Life expectancy at birth in Duchenne muscular dystrophy: A systematic review and meta-analysis. *Eur. J. Epidemiol.* **35**, 643–653 (2020).
48. J. Broomfield, M. Hill, M. Guglieri, M. Crowther, K. Abrams, Life expectancy in Duchenne muscular dystrophy. *Neurology* **97**, e2304 (2021).
49. F. Chemello, Z. Wang, H. Li, J. R. M. Anally, N. Liu, R. Bassel-Duby, E. N. Olson, Degenerative and regenerative pathways underlying Duchenne muscular dystrophy revealed by single-nucleus RNA sequencing. *Proc. Natl. Acad. Sci. U.S.A.* **117**, 29691–29701 (2020).
50. J. Juan-Mateu, L. Gonzalez-Quereda, M. J. Rodriguez, M. Baena, E. Verdura, A. Nascimento, C. Ortez, M. Baiget, P. Gallano, DMD mutations in 576 dystrophinopathy families: A step forward in genotype-phenotype correlations. *PLOS ONE* **10**, e0135189 (2015).
51. Z.-Y. Rao, M.-Y. Cai, G.-F. Yang, L.-R. He, S.-J. Mai, W.-F. Hua, Y.-J. Liao, H.-X. Deng, Y.-C. Chen, X.-Y. Guan, Y.-X. Zeng, H.-F. Kung, D. Xie, EZH2 supports ovarian carcinoma cell invasion and/or metastasis via regulation of TGF-β1 and is a predictor of outcome in ovarian carcinoma patients. *Carcinogenesis* **31**, 1576–1583 (2010).
52. F. Crea, E. M. Hurt, L. A. Mathews, S. M. Cabarcas, L. Sun, V. E. Marquez, R. Danesi, W. L. Farrar, Pharmacologic disruption of Polycomb Repressive Complex 2 inhibits tumorigenicity and tumor progression in prostate cancer. *Mol. Cancer* **10**, 40 (2011).
53. M. Smits, J. Nilsson, S. E. Mir, P. M. van der Stoop, E. Hulleman, J. M. Niers, P. C. de Witt Hamer, V. E. Marquez, J. Cloos, A. M. Krichevsky, D. P. Noske, B. A. Tannous, T. Würdinger, miR-101 is down-regulated in glioblastoma resulting in EZH2-induced proliferation, migration, and angiogenesis. *Oncotarget* **1**, 710–720 (2010).
54. X. Zhang, Y. Wang, J. Yuan, N. Li, S. Pei, J. Xu, X. Luo, C. Mao, J. Liu, T. Yu, S. Gan, Q. Zheng, Y. Liang, W. Guo, J. Qiu, G. Constantin, J. Jin, J. Qin, Y. Xiao, Macrophage/microglial Ezh2 facilitates autoimmune inflammation through inhibition of Socs3. *J. Exp. Med.* **215**, 1365–1382 (2018).
55. K. Mojumdar, F. Liang, C. Giordano, C. Lemaire, G. Danialou, T. Okazaki, J. Bourdon, M. Rafei, J. Galipeau, M. Divangahi, B. J. Petrof, Inflammatory monocytes promote progression of Duchenne muscular dystrophy and can be therapeutically targeted via CCR2. *EMBO Mol. Med.* **6**, 1476–1492 (2014).
56. S. Woodhouse, D. Pugazhendhi, P. Brien, J. M. Pell, Ezh2 maintains a key phase of muscle satellite cell expansion but does not regulate terminal differentiation. *J. Cell Sci.* **126**, 565–579 (2013).
57. Z. A. Tanoury, J. Rao, O. Tassy, B. Gobert, S. Gapon, J.-M. Garnier, E. Wagner, A. Hick, A. Hall, E. Gussoni, O. Pourquié, Differentiation of the human PAX7-positive myogenic precursors/satellite cell lineage in vitro. *Development* **147**, dev187344 (2020).
58. C. Hartmann, Y. A. Schwietzer, T. Otani, M. Furuse, K. Ebnet, Physiological functions of junctional adhesion molecules (JAMs) in tight junctions. *Biochim. Biophys. Acta Biomembr.* **1862**, 183299 (2020).
59. S. Stelzer, M. M. Worlitzer, L. Bahnassawy, K. Hemmer, K. Rugani, I. Werthschulte, A. L. Schon, B. F. Brinkmann, E. C. Bunk, T. Palm, K. Ebnet, J. C. Schwamborn, JAM-C is an apical surface marker for neural stem cells. *Stem Cells Dev.* **21**, 757–766 (2012).
60. J. P. Auger, M. Zimmermann, M. Faas, U. Stifel, D. Chambers, B. Krishnacoumar, R. V. Taudte, C. Grund, G. Erdmann, C. Scholtysek, S. Uderhardt, O. Ben Brahim, M. Pascual Mate, C. Stoll, M. Bottcher, K. Palumbo-Zerr, M. S. J. Mangan, M. Dzamukova,

M. Kieler, M. Hofmann, S. Bluml, G. Schabbauer, D. Mougiakakos, U. Sonnewald, F. Hartmann, D. Simon, A. Kleyer, A. Gruneboom, S. Finotto, E. Latz, J. Hofmann, G. Schett, J. Tuckermann, G. Kronke, Metabolic rewiring promotes anti-inflammatory effects of glucocorticoids. *Nature* **629**, 184–192 (2024).
61. R. K. Gilbert, W. A. Hawk, The incidence of necrosis of muscle fibers in Duchenne type muscular dystrophy. *Am. J. Pathol.* **43**, 107–122 (1963).
62. M. Sandri, C. Minetti, M. Pedemonte, U. Carraro, Apoptotic myonuclei in human Duchenne muscular dystrophy. *Lab. Invest.* **78**, 1005–1016 (1998).
63. S. E. Hong, J. Kneissl, A. Cho, M. J. Kim, S. Park, J. Lee, S. Woo, S. Kim, J. S. Kim, S. Y. Kim, S. Jung, J. Kim, J. Y. Shin, J. H. Chae, M. Choi, Transcriptome-based variant calling and aberrant mRNA discovery enhance diagnostic efficiency for neuromuscular diseases. *J. Med. Genet.* **59**, 1075–1081 (2022).
64. Y. Hao, S. Hao, E. Andersen-Nissen, W. M. Mauck III, S. Zheng, A. Butler, M. J. Lee, A. J. Wilk, C. Darby, M. Zager, P. Hoffman, M. Stoeckius, E. Papalexi, E. P. Mimitou, J. Jain, A. Srivastava, T. Stuart, L. M. Fleming, B. Yeung, A. J. Rogers, J. M. McElrath, C. A. Blish, R. Gottardo, P. Smibert, R. Satija, Integrated analysis of multimodal single-cell data. *Cell* **184**, 3573–3587.e29 (2021).
65. J. D. Welch, V. Kozareva, A. Ferreira, C. Vanderburg, C. Martin, E. Z. Macosko, Single-cell multi-omic integration compares and contrasts features of brain cell identity. *Cell* **177**, 1873–1887.e17 (2019).
66. S. Aibar, C. B. González-Blas, T. Moerman, V. A. Huynh-Thu, H. Imrichova, G. Hulselmans, F. Rambow, J.-C. Marine, P. Geurts, J. Aerts, J. van den Oord, Z. K. Atak, J. Wouters, S. Aerts, SCENIC: Single-cell regulatory network inference and clustering. *Nat. Methods* **14**, 1083–1086 (2017).
67. S. Jin, C. F. Guerrero-Juarez, L. Zhang, I. Chang, R. Ramos, C.-H. Kuan, P. Myung, M. V. Plikus, Q. Nie, Inference and analysis of cell-cell communication using CellChat. *Nat. Commun.* **12**, 1088 (2021).
68. K. Street, D. Risso, R. B. Fletcher, D. Das, J. Ngai, N. Yosef, E. Purdom, S. Dudoit, Slingshot: Cell lineage and pseudotime inference for single-cell transcriptomics. *BMC Genomics* **19**, 477 (2018).
69. K. Van den Berge, H. Roux de Bezieux, K. Street, W. Saelens, R. Cannoodt, Y. Saeys, S. Dudoit, L. Clement, Trajectory-based differential expression analysis for single-cell sequencing data. *Nat. Commun.* **11**, 1201 (2020).
70. N. Borcherding, A. Vishwakarma, A. P. Voigt, A. Bellizzi, J. Kaplan, K. Nepple, A. K. Salem, R. W. Jenkins, Y. Zakharia, W. Zhang, Mapping the immune environment in clear cell renal carcinoma by single-cell genomics. *Commun. Biol.* **4**, 122 (2021).
71. D. W. M. Kellar, L. D. Walter, L. T. Song, M. Mantri, M. F. Z. Wang, I. De Vlaminck, B. D. Cosgrove, Large-scale integration of single-cell transcriptomic data captures transitional progenitor states in mouse skeletal muscle regeneration. *Commun. Biol.* **4**, 1280 (2021).
72. H. J. Kok, E. R. Barton, Actions and interactions of IGF-I and MMPs during muscle regeneration. *Semin. Cell Dev. Biol.* **119**, 11–22 (2021).
73. U. Lee, P. Stuelsatz, S. Karaz, D. W. McKellar, J. Russeil, M. Deak, I. De Vlaminck, C. Lepper, B. Deplancke, B. D. Cosgrove, J. N. Feige, A Tead1-Apelin axis directs paracrine communication from myogenic to endothelial cells in skeletal muscle. *iScience* **25**, 104589 (2022).
74. A. M. Norris, A. B. Appu, C. D. Johnson, L. Y. Zhou, D. W. McKellar, M.-A. Renault, D. Hammers, B. D. Cosgrove, D. Kopinke, Hedgehog signaling via its ligand DHH acts as cell fate determinant during skeletal muscle regeneration. *Nat. Commun.* **14**, 3766 (2023).
75. R. Browaeys, W. Saelens, Y. Saeys, NicheNet: Modeling intercellular communication by linking ligands to target genes. *Nat. Methods* **17**, 159–162 (2020).
76. P. A. Ewels, A. Peltzer, S. Fillinger, H. Patel, J. Alneberg, A. Wilm, M. U. Garcia, P. Di Tommaso, S. Nahnsen, The nf-core framework for community-curated bioinformatics pipelines. *Nature Biotechnology* **38**, 276-278 (2020).
77. I. Tirosh, B. Izar, S. M. Prakadan, M. H. Wadsworth, D. Treacy, J. J. Trombetta, A. Rotem, C. Rodman, C. Lian, G. Murphy, M. Fallahi-Sichani, K. Dutton-Regester, J.-R. Lin, O. Cohen, P. Shah, D. Lu, A. S. Genshaft, T. K. Hughes, C. G. K. Ziegler, S. W. Kazer, A. Gaillard, K. E. Kolb, A.-C. Villani, C. M. Johannessen, A. Y. Andreev, E. M. Van Allen, M. Bertagnolli, P. K. Sorger, R. J. Sullivan, K. T. Flaherty, D. T. Frederick, J. Jané-Valbuena, C. H. Yoon, O. Rozenblatt-Rosen, A. K. Shalek, A. Regev, L. A. Garraway, Dissecting the multicellular ecosystem of metastatic melanoma by single-cell RNA-seq. *Science* **352**, 189–196 (2016).
78. V. Kleshchevnikov, A. Shmatko, E. Dann, A. Aivazidis, H. W. King, T. Li, R. Elmentaite, A. Lomakin, V. Kedlian, A. Gayoso, M. S. Jain, J. S. Park, L. Ramona, E. Tuck, A. Arutyunyan, R. Vento-Tormo, M. Gerstung, L. James, O. Stegle, O. A. Bayraktar, Cell2location maps fine-grained cell types in spatial transcriptomics. *Nat. Biotechnol.* **40**, 661–671 (2022).
79. W. J. Kent, C. W. Sugnet, T. S. Furey, K. M. Roskin, T. H. Pringle, A. M. Zahler, D. Haussler, The human genome browser at UCSC. *Genome Res.* **12**, 996–1006 (2002).
80. G. Yu, L.-G. Wang, Q.-Y. He, ChIPseeker: An R/Bioconductor package for ChIP peak annotation, comparison and visualization. *Bioinformatics* **31**, 2382–2383 (2015).
81. Q. Wang, M. Li, T. Wu, L. Zhan, L. Li, M. Chen, W. Xie, Z. Xie, E. Hu, S. Xu, G. Yu, Exploring epigenomic datasets by ChIPseeker. *Curr. Protoc.* **2**, e585 (2022).
82. S. Karakashev, T. Fukumoto, B. Zhao, J. Lin, S. Wu, N. Fatkhutdinov, P. H. Park, G. Semenova, S. Jean, M. G. Cadungog, M. E. Borowsky, A. V. Kossenkov, Q. Liu, R. Zhang, EZH2 inhibition sensitizes CARM1-high, homologous recombination proficient ovarian cancers to PARP inhibition. *Cancer Cell* **37**, 157–167.e6 (2020).
83. R. T. Kurmasheva, M. Sammons, E. Favours, J. Wu, D. Kurmashev, K. Cosmopoulos, H. Keilhack, C. R. Klaus, P. J. Houghton, M. A. Smith, Initial testing (stage 1) of tazemetostat (EPZ-6438), a novel EZH2 inhibitor, by the Pediatric Preclinical Testing Program. *Pediatr. Blood Cancer* **64**, e26218 (2017).
84. X. Huang, J. Yan, M. Zhang, Y. Wang, Y. Chen, X. Fu, R. Wei, X. L. Zheng, Z. Liu, X. Zhang, H. Yang, B. Hao, Y. Y. Shen, Y. Su, X. Cong, M. Huang, M. Tan, J. Ding, M. Geng, Targeting epigenetic crosstalk as a therapeutic strategy for EZH2-aberrant solid tumors. *Cell* **175**, 186–199.e19 (2018).
85. MedChemExpress, Deflazacort (MedChemExpress); https://www.medchemexpress.com/Deflazacort.html?srsltid=AfmBOopwXuzWJFXh6XZz1vzq5x1J6NinpMnPr4yJy1mjwlz3Ft0Fk-T7.
86. C. Stringer, M. Pachitariu, Cellpose3: One-click image restoration for improved cellular segmentation. bioRxiv 579780 [Preprint] (2024). https://doi.org/10.1101/2024.02.10.579780.
87. C. Long, L. Amoasii, A. A. Mireault, J. R. McAnally, H. Li, E. Sanchez-Ortiz, S. Bhattacharyya, J. M. Shelton, R. Bassel-Duby, E. N. Olson, Postnatal genome editing partially restores dystrophin expression in a mouse model of muscular dystrophy. *Science* **351**, 400–403 (2016).
88. P. P. Laurila, P. Luan, M. Wohlwend, N. Zanou, B. Crisol, T. de Imamura Lima, L. J. E. Goeminne, H. Gallart-Ayala, M. Shong, J. Ivanisevic, N. Place, J. Auwerx, Inhibition of sphingolipid de novo synthesis counteracts muscular dystrophy. *Sci. Adv.* **8**, eabh4423 (2022).

Acknowledgments: We express our gratitude to all of the muscle donors and their families for their participation. We thank Y.-Y. Kong and J.-S. Kang for assistance with muscle dissection and M. Petitjean, L. Chen, and A. Lightstone at FibroNest for assistance with quantitative AI digital pathology image analysis. **Funding:** This work was supported in part by grants from the Korean Research Foundation (RS-2023-00223069 to M.C., J.-H.C., C.-H.L., and I.J.) and by the SNUH Lee Kun-Hee Child Cancer & Rare Disease Project, Republic of Korea (22B-001-0500 to J.-H.C. and M.C.). **Author contributions:** Conceptualization: M.C., J.-H.C., C.-H.L., and A.C. Methodology: E.Y.J., Y.K., R.G.K., J.-K.W., A.C., I.J., C.-H.L., and J.P. Software: E.Y.J., Y.K., and J.P. Validation: E.Y.J., Y.K., H.Kang, I.J., C.-H.L., and J.P. Formal analysis: E.Y.J., Y.K., J.-K.W., A.C., C.-H.L., and J.P. Investigation: E.Y.J., Y.K., H.Kang, H.Kim, S.Y.J., S.P., A.C., I.J., and J.P. Resources: E.Y.J., H.Kang, S.P., D.K., A.C., I.J., C.-H.L., H.-Y.K., J.-H.C., and M.C. Data curation: E.Y.J., A.C., C.-H.L., and J.-H.C. Writing—original draft: E.Y.J., H.Kang, C.-H.L., J.-H.C., and M.C. Writing—review and editing: E.Y.J., Y.K., H.Kang, R.G.K., D.K., A.C., I.J., C.-H.L., J.P., H.-Y.K., J.-H.C., and M.C. Visualization: E.Y.J., H.Kang, A.C., I.J., C.-H.L., and M.C. Supervision: M.C., J.-H.C., J.P., C.-H.L., I.J., and A.C. Project administration: E.Y.J., C.-H.L., J.-H.C., and M.C. Funding acquisition: M.C., J.-H.C., and C.-H.L. **Competing interests:** The authors (E.J., J.-H.C., and M.C.) disclose that a patent application (Korean Patent Application No. 10-2024-0096174, filed on 22 July 2024) related to the findings in this manuscript is currently pending. The other authors declare that they have no competing interests. **Data and materials availability:** All data needed to evaluate the conclusions in the paper are present in the paper and/or the Supplementary Materials. All codes used in the analysis can be found at https://doi.org/10.5281/zenodo.14021079. Human and mouse 10x snRNA-seq used in the study are available at the NCBI GEO with accession numbers GSE288958 and GSE289040. 10x Genomics Visium data used in the study are available at the NCBI SRA with accession number PRJNA1218493. Vizgen MERFISH spatial transcriptomics data used in the study are available at the Korea BioData Station with accession number KAP240791.

Submitted 2 July 2024
Accepted 10 February 2025
Published 14 March 2025
10.1126/sciadv.adr4443